OPEN ACCESS

The Impact of CO_2 Evolved from VC and FEC during Formation of Graphite Anodes in Lithium-Ion Batteries

To cite this article: K. Uta Schwenke *et al* 2019 *J. Electrochem. Soc.* **166** A2035

View the article online for updates and enhancements.

The Impact of CO₂ Evolved from VC and FEC during Formation of Graphite Anodes in Lithium-Ion Batteries

K. Uta Schwenke,[1,=,z] Sophie Solchenbach,[1,=,*] Julien Demeaux,[2] Brett L. Lucht,[2,*] and Hubert A. Gasteiger[1,**]

[1]*Chair of Technical Electrochemistry, Department of Chemistry and Catalysis Research Center, Technical University of Munich, Munich, Germany*
[2]*Department of Chemistry, University of Rhode Island, Kingston, Rhode Island, USA*

Additives such as vinylene carbonate (VC) and fluoroethylene carbonate (FEC) are commonly added to lithium-ion battery electrolytes in order to form a solid electrolyte interphase (SEI) on the anode, suppressing continuous solvent reduction. In this work, we directly compare VC and FEC by analyzing the SEI with FTIR and XPS, and the evolved gases with on-line electrochemical mass spectrometry (OEMS) in different model systems. Since both additives evolve mainly CO₂ during formation, the effect of CO₂ as an additive is compared to the addition of VC and FEC. While Li₂CO₃ is as expected the main SEI compound found due to the added CO₂, surprisingly no CO was detected in the gas phase of such cells. Based on FTIR, NMR and OEMS analyses of cells filled with ¹³C labeled CO₂, we suggest a mechanism explaining the beneficial effects of CO₂ and hence also of CO₂ evolving additives in lithium-ion battery cells. While the generation of polycarbonate from FEC or VC reduction is observed, the generation of Li₂CO₃ may be as important as the generation of polycarbonate.

The solid electrolyte interphase (SEI),[1] which is formed on the anode of a lithium-ion battery during the initial cycle(s), provides electrical passivation and lithium ion conduction and thus allows stable lithium ion intercalation without further electrolyte reduction. A typical electrolyte consists of LiPF₆ in a mixture of cyclic (e.g., ethylene carbonate (EC)) and linear alkyl carbonates (e.g., ethyl methyl carbonate (EMC)). To tailor the SEI for more efficient protection against continuous solvent reduction, additives such as vinylene carbonate (VC) or fluoroethylene carbonate (FEC) are added to the electrolyte. Both additives are reduced at higher potentials than the standard electrolyte,[2] which prevents the reduction of the main electrolyte components. While VC has been established as a standard additive for graphite-based cell chemistries, FEC is commonly used in combination with silicon anodes.[3–8]

In a movement toward a rational design of electrolyte additives, the decomposition mechanisms and products of additives have been studied thoroughly. Regarding VC and FEC, both additives are known to form polymer species during reduction.[4,7,9–11] The decomposition of FEC is often also related to an enhanced formation of LiF.[2,6,8,12] Besides, the use of FEC with silicon anodes in contrast to VC on graphite electrodes makes a direct comparison of these two additives more difficult. Still, it is often overlooked that both additives have been reported to release CO₂ during reduction.[10,13–15] CO₂ has been used as one of the first SEI-forming additives in lithium metal and lithium ion batteries with graphite anodes.[16–25] Recently, Krause et al. demonstrated the beneficial effect of CO₂ as a cycle life extending additive in full pouch cells with silicon alloy anodes.[26] Our group recently showed that CO₂ reduces the FEC consumption in silicon-graphite based full-cells,[27] and can stop the ester exchange reactions caused by lithium alkoxide species,[28] which are a product of the reduction of linear carbonates.[29]

In this work, we investigate the effect of VC and FEC on the SEI composition of graphite electrodes using surface sensitive analytical techniques such as XPS and FTIR spectroscopy. Using different model electrolytes, we take a closer look into the origin of LiF in the SEI. We analyze further the potential-resolved gassing behavior of both VC and FEC. As the gas evolution pattern of both additives shows that CO₂ can also be consumed at low potentials, we investigate the

consumption of CO₂ and its effect on the SEI composition. By introducing isotopically labeled ¹³CO₂ in the cell's head space, we are able to differentiate between electrolyte decomposition products and products of the CO₂ reduction. Thus, with the combination of FTIR, NMR and OEMS analysis, we elucidate the multi-step CO₂ reduction mechanism occurring on graphite electrodes.

Experimental

Electrode preparation.—Graphite electrodes were prepared by mixing SLP30 graphite powder (Timcal, Switzerland, BET surface area 7 m²/g) with polyvinylidene fluoride binder (PVDF, Kynar HSV900, Arkema, France) at a weight ratio of 90/10 in N-methyl-2-pyrrolidone (NMP, anhydrous, 99.5%, Sigma-Aldrich, Germany). The obtained slurry with a solid content of 33% was mixed for 15 min at 2000 rpm in a planetary orbital mixer (ARV-310CE, Thinky, USA) and coated with a gap bar onto either a copper foil (thickness 12 μm, MTI Corporation, USA) or a porous separator (H2013, Celgard, USA or FS24316, Freudenberg, Germany) at a wet-film thickness of 250 μm using an automatic coater (RK PrintCoat Instruments, UK). The coating was dried at 50°C before punching it with a precision punch (Hohsen, Japan) into 15 mm diameter disks and final drying under dynamic vacuum in a glass oven (drying oven 585, Büchi, Switzerland) at 120°C (for coatings on copper foil or Freudenberg separator) or at 95°C (for coatings on Celgard separator). The final electrodes had a loading of ≈6 mg₍graphite₎/cm².

LFP electrodes were prepared by mixing lithium iron phosphate powder (LFP with a carbon coating of 1.9%, Clariant, Germany), PVDF (Solef 5130, Solvay, Germany), Super C65 carbon black (Timcal, Switzerland) and vapor grown carbon fibers (VGCF-H, Showa Denko, USA) at a weight ratio of 80/10/5/5 with NMP (solid content 33%) in a planetary orbital mixer (15 min at 2000 rpm). The ink was coated with a gap bar onto aluminum foil (thickness 18 μm, MTI corporation, USA) at a wet-film thickness of 500 μm using the automatic coater. The coating was dried at 50°C before punching it with a precision punch into 14 mm disks and final drying under dynamic vacuum at 120°C. The final electrodes had a loading of ≈12 mg₍LFP₎/cm², which results in an anode/cathode capacity ratio of ≈1.1. Based on a theoretical capacity of 170 mAh/g₍LFP₎, the areal capacity of the employed LFP electrodes was hence around 2 mAh/cm².

=These authors contributed equally to this work.
*Electrochemical Society Member.
**Electrochemical Society Fellow.
zE-mail: uta.schwenke@tum.de

Electrochemical cycling.—In order to investigate the influence of CO_2 on the SEI formation, cells must be used which can be filled with gases. Hence, we employed for the study at hand our home-made cell design originally developed for Li-air battery cell studies.[30] Electrolyte solutions of 1 M $LiPF_6$ (BASF) in a mixture of propylene carbonate and ethylene carbonate (PC/EMC, 30/70 by weight, Selectilyte, BASF) were employed to quickly judge whether with the respective additive a stable SEI is formed, which would suppress the otherwise continuous PC intercalation and reduction.

All cells were assembled in an argon filled glove box ($O_2 <0.1$ ppm, $H_2O <0.1$ ppm, MBraun, Germany). When building full-cells, LFP electrodes were placed onto the flat bottom part of the cell, followed by 40 µl of electrolyte, 2 Celgard separators H2013, another 40 µl of electrolyte and a graphite electrode coated on a H2013 separator (coated side facing the gas phase), followed by a final 40 µl of electrolyte and a steel mesh (21 mm diameter, 0.22 mm diameter wire, 1.0 mm openings, Spörl KG, Germany) as current collector. In order to study the effect of CO_2, cells were flushed for 35 s at a flow of 15 Nl/h with CO_2 (99.995%, Westfalen, Germany). For comparison, standard 2032 coin cells with graphite electrodes coated on copper and filled with 60 µl of electrolyte were assembled for cells without CO_2 filling.

After 1 h rest at open circuit voltage, the cells were galvanostatically cycled at 25°C in a climate chamber (Binder, Germany) with a battery cycler (Series 4000, Maccor, USA) between 2.7 and 3.8 V at rates of C/20 (1st cycle) and C/10 (2nd and 3rd cycle), followed by 37 cycles at C/5 without a constant voltage step.

Surface analysis with FTIR, XPS and NMR.—Surface characterization of graphite electrodes was conducted after one formation cycle at C/20 at 25°C between 2.7 and 3.9 V with a potentiostat (VMP3, Biologic, France), using the Li-air cell design for those type of experiments. All cells were either flushed with 1 atm CO_2 or with argon in order to avoid any contamination from remaining CO_2 from the glove box. Cells with $^{13}CO_2$ were filled via a diffusion procedure. An empty Li-air cell and the assembled, gas-flushed cell to be filled with $^{13}CO_2$ were connected via a Swagelok assembly with a valve between them. The empty cell was evacuated for 1 h and then filled with 1 atm $^{13}CO_2$ (Sigma-Aldrich, 99% chemical purity, 99% isotope purity) while the valve between the cells remained closed. Afterwards, the valve to the connected assembled cell was opened to allow intermixing of the gas volumes for 1 h, resulting in approximately 50% $^{13}CO_2$ in the cell headspace.

Electrodes were harvested from cells with standard electrolyte LP57 (EC:EMC 3:7 (w:w), 1 M $LiPF_6$, Selectilyte, BASF) or for more specific analysis with pure single solvent electrolytes. Cells with LP57 and 1 M $LiPF_6$ in EMC were assembled with graphite electrodes coated on H2013 Celgard separator and the same separator; cells with 1 M $LiPF_6$ in EC, VC or FEC were assembled with electrodes coated on Freudenberg separator FS24316 and the same separator, as those solvents could not wet the H2013 separator.

After the formation cycle, cells were flushed with argon and transferred in an argon-filled glove box. The graphite electrodes were harvested, rinsed with 3 × 0.5 ml dimethyl carbonate (DMC, 99.9%, anhydrous, Sigma-Aldrich, stored over molecular sieves), subsequently dried for approximately 5 h under dynamic vacuum in a glass oven at room temperature and brought back to the glove box without any exposure to air.

Fourier transform infrared spectroscopic (FTIR) analysis was conducted in the glove box with a MIRacle germanium ATR (Pike Technologies) incorporated in the FTIR spectrometer Spectrum Two (Perkin Elmer) with a resolution of 4 cm^{-1}. The spectra are shown as recorded without normalization.

X-ray photoelectron spectroscopy (XPS) analysis was conducted with a K-alpha spectrometer (Thermo Fisher Scientific) using a pass energy of 50 eV. All electrodes were cut in the glove box and mounted on an air-tight sample holder with metal clips to avoid any contact with air and glue. The binding energy of the obtained spectra was corrected to the F1s core spectrum of LiF at 685.0 eV. The relative atomic concentration of each element was obtained based on peak areas and sensitivity factors using the Thermo Avantage software.

NMR analysis was conducted of D_2O extracts of the graphite electrodes. The SEI components were dissolved by adding 550 µl of D_2O (99 atom % D in ampoules, Sigma-Aldrich) to the electrode and storing it for 30 min in the glove box before transferring the solution in an air-tight NMR tube (Screw Cap Tubes, Wilmad). ^1H, ^{19}F and ^{31}P NMR spectra were collected on a Bruker Ascend 400 (400 MHz) NMR spectrometer without proton decoupling, accumulating 128, 128 and 256 scans, respectively. ^{13}C NMR spectra were collected with and without proton decoupling on a Bruker Avance-III (500 MHz, equipped with a cryo probe 5 mm CPQNP), accumulating 2500 scans. For quantification, standard solutions of deuterated sodium trimethylsilyl propanoate (TSP) in D_2O (10 µl of 0.05 w.-% TSP in D_2O for ^1H NMR, 100 µl of 0.75 w.-% TSP in D_2O for ^{13}C NMR) were added to the samples in the glove box. ^{13}C NMR spectra for quantification were measured with an increased relaxation time T1 of 100 s and 350 scans to ensure complete relaxation of the spins of Li_2CO_3.

On-Line electrochemical mass spectrometry (OEMS).—For OEMS analysis, high surface area carbon black model electrodes were prepared in order to minimize lithium intercalation and maximize the signals of the evolved gases. Super C65 carbon black (Timcal, Switzerland, BET surface area 68 m^2/g) was mixed with PVDF (Kynar HSV900, Arkema, France) at a 90/10 weight ratio in NMP with a planetary orbital mixer. The obtained slurry was coated on a polyester separator (Freudenberg FS 24316) with a gap bar (500 µm). The coating was dried at 50°C before punching into 15 mm disks and drying under dynamic vacuum at 120°C. The final electrodes had a loading of 1.8 mg_{carbon}/cm^2.

To avoid any crosstalk of the evolved gases with the lithium counter electrode, OEMS analysis[31] was conducted in our recently developed 2-compartment cell[32] that employs a lithium ion conducting glass ceramic (LICGC, diameter 1'', thickness 150 µm, 10^{-4} S/cm at 25°C, Ohara, Japan) with an improved aluminum sealing.[33] In order to assign the evolved gases to the different components of the electrolyte, we employed 1 M $LiPF_6$ in pure VC, FEC, EMC or EC (all Selectilyte, BASF). As a model electrolyte, also 0.5 M LiTFSI (BASF) in diglyme (anhydrous, Sigma-Aldrich, Germany) was used. The counter electrode compartment, which is shielded from the OEMS inlet, contained the Li counter electrode (ø 17 mm, 450 µm thickness, 99.9%, Rockwood Lithium, USA) and a 22 mm diameter glass fiber separator soaked with 200 µl electrolyte. The working electrode compartment that is connected to the OEMS inlet contained the C65 working electrode (ø 15 mm) and a polyester separator (ø 17 mm) soaked with 100 µl electrolyte. The cells were connected to the OEMS system and purged for 45 s with pure argon to remove any residual trace gases from the glove box atmosphere. After an OCV period of 4 h, the carbon working electrodes were polarized from OCV ($\sim$3 V) to 0.1 V and back to 2 V with a scan rate of 0.1 mV/s. All mass spectrometer currents were normalized to the current at m/z = 36 (Ar isotope) in order to correct for minor pressure and temperature deviations, and afterwards the currents m/z = 2 (H_2), m/z = 26 (C_2H_4), m/z = 28 (CO, corrected for contributions from C_2H_4 and CO_2 as described by Strehle et al.[28]), and m/z = 44 (CO_2) were converted into gas concentrations using a calibration gas containing H_2, O_2, CO_2, and C_2H_4 (each 2000 ppm) or H_2, O_2, CO_2, and CO (each 2000 ppm).

Cells with $^{13}CO_2$ were filled via a diffusion procedure similar to the cells for surface analysis. First, the cell was purged with pure argon for 45 s to remove any residual trace gases from the glove box atmosphere. A stainless steel tube ($\sim$5 ml volume) was connected to the cell, evacuated for 30 min and then filled with $^{13}CO_2$. Then, the valve between the tube and the cell was opened to allow intermixing of the gas volumes for 30 min, resulting in 10%–30% $^{13}CO_2$ in the cell headspace. The exact headspace concentration of $^{13}CO_2$ in each cell was determined by quantification of the m/z = 45 current during the 4 h OCV period prior to the voltage sweep, assuming the same calibration factor as for $^{12}CO_2$ on m/z = 44.
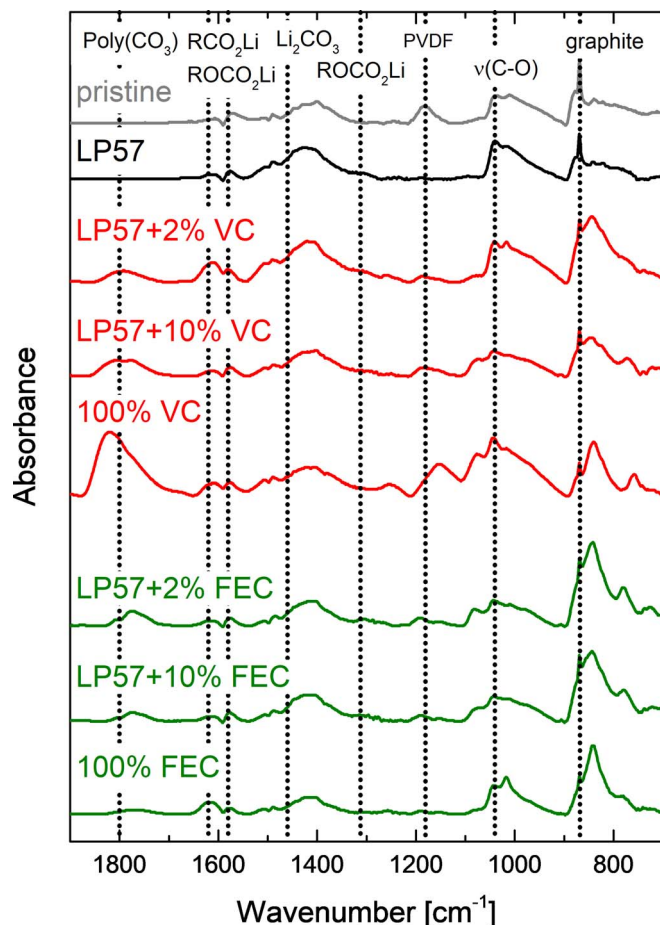
Figure 1. ATR-FTIR spectra of PVDF-bonded graphite electrodes after one formation cycle at C/20 between 2.7 and 3.9 V in 1 M LiPF$_6$ in EC/EMC (3:7, LP57) with various amounts of VC (red lines) and FEC (green lines) ranging from 0–100%. The spectrum nominated "pristine" consists of a pristine graphite electrode.

Results

SEI formation in dependence of VC and FEC concentration.— Ex situ surface analysis of cycled electrodes is commonly applied to determine the composition of the SEI and draw conclusions about the formation mechanism, whereby FTIR analysis is one of the most convenient and simplest techniques to use. Therefore, we started our comparative study of VC and FEC as SEI additives for graphite anodes using ATR-FTIR analysis. The corresponding spectra of graphite electrodes after one formation cycle (at C/20 between 2.7 and 3.9 V) in standard LP57 electrolyte with different amounts of VC and FEC additive are displayed in Figure 1. Although the additive content varied from 0% to 100%, only very few changes among the electrodes were observed. All electrodes showed bands from stretching vibrations characteristic for Li$_2$CO$_3$ (around 1460 cm^{-1}), alkyl carbonates (around 1620 and 1310 cm^{-1}) and carboxylates (around 1580 cm^{-1}). The only major difference occurring due to the additives in comparison to the standard electrolyte consists of a band around 1800 cm^{-1}, which was attributed to the stretching vibration of the carbonyl group of poly(VC).[9] A similar band is observed for the SEI formed with FEC. Interestingly, the intensity of this band is independent of the FEC concentration, whereas the poly(VC) band increases strongly with VC concentration.

The similarities between the observed reduction products of VC and FEC led in the literature to the suggestion that FEC transforms to VC and finally forms also poly(VC).[4,11] Theoretical studies also suggested that FEC and VC reduction may lead to the same reduction

products.[34] However, a single IR-band is not sufficient to identify a SEI product, and a carbonyl stretching vibration at such high wavenumbers suggests only that the vibration is quite constrained, as for example would also be the case in non-polymeric cyclic carbonates. As a product remaining in the SEI must be a non-soluble solid, it is commonly assumed that also in the case of FEC a polymer with a constrained carbonyl group is formed, which was named either poly(FEC)[2,8] or was directly assigned to be poly(VC).[4,11] An identical product as in the case of VC is unlikely, as the vibration around 1800 cm^{-1} occurs at a slightly lower wavenumber for FEC than for VC (see Figure 1).

Interestingly, this poly(FEC) is only formed in small quantities, independent of the FEC concentration, in contrast to poly(VC), whose amount increases strongly with VC concentration (see Figure 1). This finding explains why FEC can be added to electrolytes as a co-solvent, whereas the amount of VC has to be well-dosed to avoid the uncontrolled formation of a poorly ion conducting polymer, which leads to high cell impedance.[35–37] As the poly(FEC) concentration is observed to be independent of the initial FEC concentration after the 1st cycle (see Figure 1), the formation of poly(FEC) seems to involve an electron transfer, which is no longer possible after a certain SEI layer thickness has been reached. Nie et al.[5] analyzed the SEI on silicon electrodes after 1, 5 and 20 cycles in a pure single-solvent FEC electrolyte and showed that the amount of poly(FEC) increased for those electrodes with cycle number. This might be one important reason why FEC is the preferred additive for silicon anodes for which the SEI has to be reformed in each cycle, until all FEC is consumed and the cycling performance drops.[14,38]

The origin of LiF in the SEI.—Next to FTIR spectroscopy, XPS is commonly employed to analyze the SEI. Numerous studies exist to identify components formed due to the reductive decomposition of VC[9,10,39,40] or FEC,[3–6,41,42] which are the basis of a variety of suggested mechanisms. Since one major difference between VC and FEC is the additional fluorine, it seems obvious that in case of FEC, more LiF should be found on the anode. Indeed, several studies show that more LiF forms on electrodes cycled in FEC containing electrolytes compared to standard electrolytes without FEC.[3,8,41–43] Other articles report, however, no difference in fluorine concentration[2,4] or even a lowered amount when using a FEC containing electrolyte.[44] Whether the effect of LiF in the SEI is positive or negative is under debate: On the one hand, the lithium ion conductivity is relatively low compared to other lithium salts in the SEI;[39,45] on the other hand, it was found that carbon electrodes with fluorinated binders like PTFE or PVDF cycle in a more stable manner than with fluorine-free binders like EPDM, which was attributed to the formation of LiF.[19] Moreover, LiPF$_6$, the most widely-used Li-ion battery electrolyte salt, is known for the formation of LiF,[46,47] which is thus a common and probably also important part of the SEI.

In this study, we use XPS to investigate the effect of VC, FEC and also LiPF$_6$ on the formation of LiF. Figure 2a shows the ratios of different elements in the SEI of graphite electrodes after formation in different electrolytes determined by XPS. While the analysis of the core spectra of carbon and oxygen leaves room for interpretation, depending on the number and position of the peaks used for fitting, the F1s peak of LiF at 685 eV can be easily distinguished from other fluorine containing species with C-F or P-F bonds, such as PVDF or LiPF$_6$ with binding energies around 687/688 eV. Therefore, we additionally deconvoluted the ratio of LiF (dark blue) from the other fluorine species (light blue) in Figure 2a.

First, we employed model electrolytes containing only 1 M LiPF$_6$ in EMC ((1) in Figure 2a), to which 2% of VC (2) or FEC (3) were added. As can be seen in Figure 2a, the addition of VC (2) suppressed the decomposition of LiPF$_6$ efficiently and the resulting SEI contained less LiF in comparison to the additive-free electrolyte (1) (6% vs. 13%), as already reported in the literature.[2,8,39] In contrast, the amount of LiF was approximately doubled (28%) when using FEC (3). Interestingly, the elemental composition and also the amount of LiF were surprisingly similar between the standard electrolyte LP57 with EC (5) and the model electrolyte with EMC only (1).
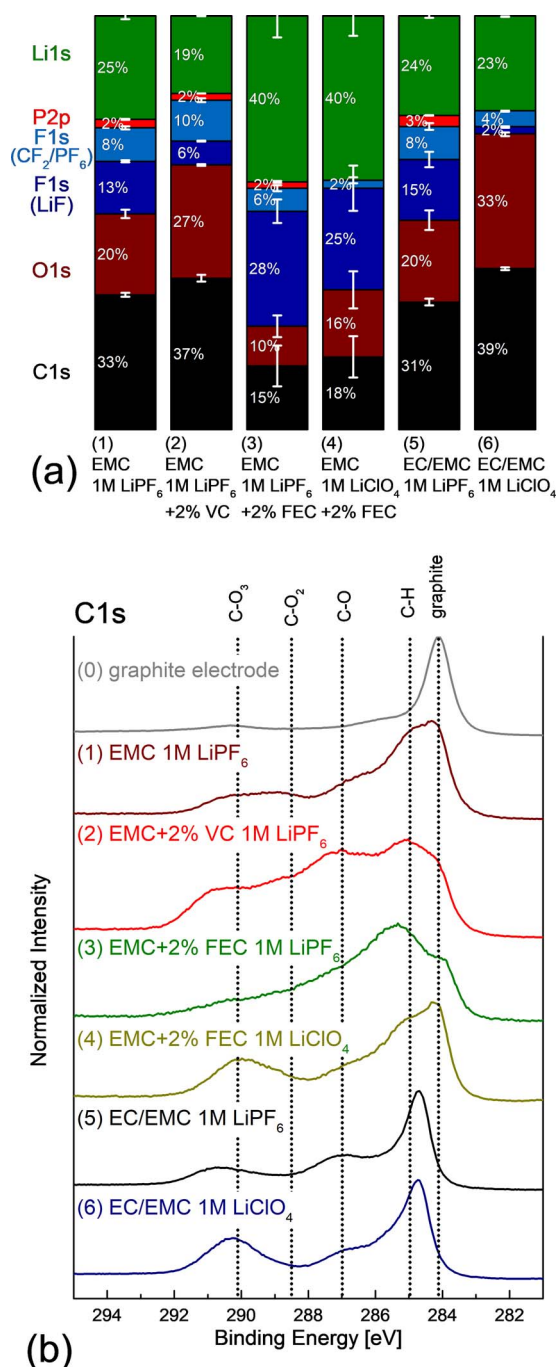
Figure 2. XPS analysis of PVDF-bonded graphite electrodes after one formation cycle at C/20 between 2.7 and 3.9 V versus LFP in various electrolyte solutions with either 1 M LiPF$_6$ or LiClO$_4$ as salt and either EC/EMC or EMC with and without 2% additive as solvent. (a) Molar percentage of the different elements detected by XPS. Molar fractions of F bound in LiF and in C-F/P-F bonds are given separately. The error bars represent the standard deviation of several measurement points on the same electrode. Usually 2 points per electrode were measured. As the deviation for the electrode cycled in EMC+FEC was comparably high, 4 (LiPF$_6$) and 7 (LiClO$_4$) points were analyzed for these electrodes. (b) C1s core spectra normalized between 0 and 1.

In order to understand how much LiF is formed by LiPF$_6$ and PVDF, we analyzed also an electrode cycled in an electrolyte with FEC but with LiClO$_4$ instead of LiPF$_6$ (4) and one electrode with neither FEC nor LiPF$_6$ (6). Please note that we could not use the model electrolyte with only EMC as solvent when LiPF$_6$ was replaced with LiClO$_4$, as LFP/graphite cells with EMC and LiClO$_4$ without additives

never reached the upper cutoff potential, but charged without end. This behavior already indicates that LiF formed from LiPF$_6$ is an essential component of the SEI, at least when no other passivating components are available. When the LiClO$_4$-electrolyte was employed with additional EC to form a stable SEI, 2% LiF was still found by XPS, even without FEC and LiPF$_6$ (6). This demonstrates that also PVDF is unstable at the applied potentials and participates in the SEI formation, as demonstrated in the early days of Li-ion battery research.[19] However, as significantly less LiF is found in the SEI of cells with LiClO$_4$ and no additives (6) compared to the same electrolyte with LiPF$_6$ (5) (2% vs. 15%), LiPF$_6$ decomposition is indeed the main source of LiF in additive-free cells. In contrast, with LiClO$_4$ and FEC (4) almost the same amount of LiF was found as with LiPF$_6$ and FEC (3) (25% vs. 28%). This finding shows that the decomposition of LiPF$_6$ is suppressed by FEC, similar as observed for VC (2). Yet, the additional 3% of LiF found in EMC+2% FEC with LiPF$_6$ (3) might stem from the decomposition of LiPF$_6$.

To explain the presence of LiF, Markevich et al.[6] suggested a mechanism in which LiF forms exclusively via transformation of Li$_2$CO$_3$ with LiPF$_6$. Although it becomes clear from our results that the LiF in FEC-containing electrolytes originates mostly from FEC, we took a closer look at the amounts of Li$_2$CO$_3$ and LiF in the SEI of the different electrolytes. Figure 2b displays the core C1s spectra of the same electrodes as in Figure 2a. Interestingly, more carbonate (binding energy 290 eV) was found on the surface after cycling in an electrolyte with LiClO$_4$ in comparison to a LiPF$_6$ containing electrolyte. As the FTIR spectra (not shown) do not present a significant difference in the amount of Li$_2$CO$_3$, this difference seems to be highly surface sensitive. Only the top layer of the SEI, which is probed by XPS, may undergo a change from Li$_2$CO$_3$ to LiF in a LiPF$_6$ containing electrolyte. When VC is added to the electrolyte the characteristic peaks for poly(VC) at 291 and 187.5 eV were observed as expected.[9,40,48] Furthermore, it is confirmed that the SEI of electrodes after one formation cycle in an electrolyte without EC is quite thin, as the graphite peak at 284.1 eV is clearly visible, whereas the spectra of electrodes after one cycle in EC are showing dominantly peaks characteristic for alkyl carbonates at 284.8 eV, 287.1 eV and 290.7 eV, covering the graphite completely.[9,49]

In summary, we can draw the following conclusions from the here conducted XPS study: LiF is an essential part of the SEI which can be found in all electrodes. The lowest amount (2%) is obtained when neither FEC nor LiPF$_6$ are present in the electrolyte, and hence LiF originates from the decomposition of the binder PVDF. Approximately 15% of LiF is observed in the SEI of electrodes after a cycle in an electrolyte without additives but with LiPF$_6$. The addition of VC, which gets reduced at high potentials, suppresses the formation of LiF to 6%, whereas FEC in the electrolyte is the main source of LiF on electrodes as the amount of LiF is around 25%, almost independent whether LiPF$_6$ or LiClO$_4$ is used as electrolyte salt.

Gas evolution during the reductive decomposition of VC and FEC.—To further investigate the onset and the products of the decomposition of VC and FEC, we performed potential-resolved OEMS measurements in a sealed 2-compartment cell[33] in a pure VC or FEC electrolyte with 1 M LiPF$_6$. Figures 3a and 3b show the current density (upper panel) and the gas evolution (lower panel) during a reductive CV on a carbon black electrode in VC+1 M LiPF$_6$ and FEC+1 M LiPF$_6$ electrolyte, respectively. Both current density and gas evolution are normalized to the BET area of the carbon black working electrode (left y-axis) to be comparable throughout the following datasets. In the VC-only electrolyte, CO$_2$ starts to evolve around 2.2 V vs. Li$^+$/Li and rises steeply up to a maximum of 30 μmol/m$^2_{BET}$ around 1.1 V vs. Li$^+$/Li. Interestingly, no clear current peak can be associated with the strong gas evolution. The CO$_2$ evolution of the FEC-only electrolyte starts at a lower potential (1.8 V vs. Li$^+$/Li), but increases even steeper up to 40 μmol/m$^2_{BET}$ at 0.9 V. In contrast to the VC electrolyte, there is a large reduction current with a maximum at 1.1 V vs. Li$^+$/Li for FEC, coinciding with the maximum rate of CO$_2$ evolution. The difference in reduction current for VC and FEC is consistent with previous
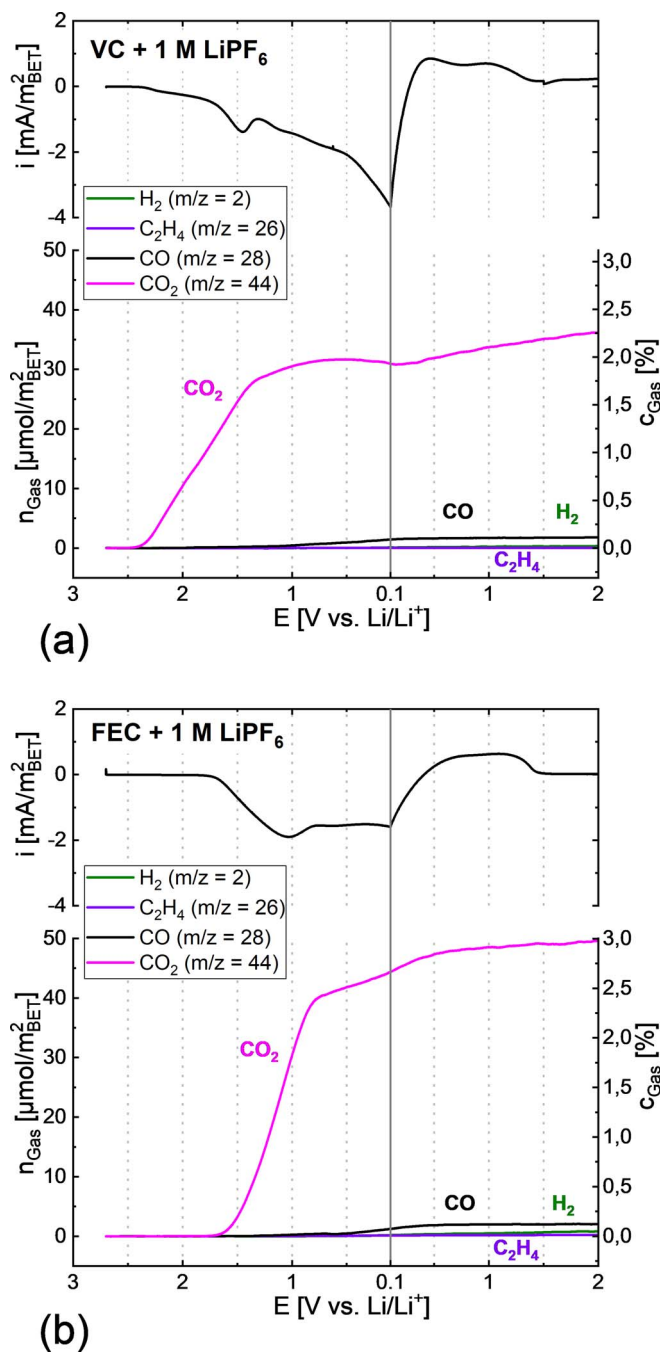
Figure 3. Gas evolution of a Super C65 carbon electrode during one CV cycle at 0.1 mV/s in two model electrolytes with 1 M $LiPF_6$ in (a) VC or in (b) FEC. The carbon working electrode is separated from the metallic lithium counter electrode with an aluminum sealed solid electrolyte diffusion barrier in the here used 2-compartment OEMS cells.

reports suggesting that VC decomposition is catalytic while FEC reduction is stoichiometric.[11] Between 1 and 0.1 V vs. Li^+/Li, the CO_2 concentration decreases slightly in the VC electrolyte, while in the FEC electrolyte CO_2 evolution is slowed down (but not stopped). At the same time, a minor amount of CO is evolved in both experiments. During the positive going scan, the CO_2 evolution increases again linearly for the VC-only electrolyte, whereas it flattens for FEC. Hydrogen and ethylene stay below the detection limit during the entire scan in both VC and FEC.

CO_2 has been previously identified as the major gaseous product of VC reduction,[9,10] and here we confirm that indeed no other species like

acetylene, which would be the equivalent to ethylene from EC reduction, are evolved. Also FEC is reported to release CO_2 during reduction on both graphite[15] and silicon,[14] while simultaneously forming LiF.[50] Recently, calculations by Soto et al.[51] have confirmed that the decarboxylated radical anion of a reduced VC molecule could be the starting point for a VC polymerization. The CO_2 evolution observed for VC which continues after the end of the reductive CV scan could belong to a chemical chain reaction which eliminates CO_2.[10,51] In contrast, almost all CO_2 released from FEC is connected to a corresponding current. This observation fits well to the abovementioned differences of VC and FEC at different concentrations (see Figure 1). However, as both poly(VC) and poly(FEC) contain intact carbonate moieties, they therefore must be produced by a decomposition pathway proceeding without any CO_2 evolution.

The change in CO_2 evolution slope between 1 and 0.1 V vs. Li^+/Li in both electrolytes points toward a CO_2-consuming process occurring at low potentials, superimposing the CO_2 evolution. Aurbach et al.[18] suggested that CO_2 can be reduced to CO and Li_2CO_3 in lithium-ion battery electrolytes. In both VC and FEC, the CO evolution starts simultaneously with the consumption of CO_2, although the amount of CO seems too little to quantitatively account for the consumed CO_2. Alternatively, CO could result from the direct 2-electron reduction of VC[52] or FEC.[53]

Since both VC and FEC reduction are characterized by a strong CO_2 evolution, and since in both cases CO_2 is partially consumed or its evolution suppressed at low potentials (< 0.8 V), we further want to investigate how (i) the presence of CO_2 affects the formation of graphite electrodes and (ii) if CO_2 plays a role in the ability of these additives to form a highly effective SEI.

Cycling in PC/EMC based electrolytes with VC, FEC and CO_2.— Even though there is a clear difference between the additives VC and FEC in terms of LiF and surface polymer formation, the previous section clearly demonstrated the similar gas evolution pattern during their initial decomposition. In order to investigate whether the evolved and possibly also consumed CO_2 plays a role in the performance and effectiveness of these two SEI forming additives, the cycling performance of cells with VC or FEC were directly compared to cells filled with gaseous CO_2. Since the cycling stability of cells with a standard EC containing electrolyte is rather high even in the absence of SEI forming additives, the effectiveness of SEI forming additives can be determined more easily by cycling cells in EC-free electrolyte. Thus, graphite/LFP cells were built with a 1 M $LiPF_6$ in PC/EMC (30/70 by weight) electrolyte with 2% VC, 2% FEC, 1 atm CO_2 or no additive at all, and cycled with a rate of C/5 after 1 formation cycle at C/20 and 2 formation cycles at C/10. Figure 4a displays the specific charge capacity versus cycle number for different electrolyte formulations. No stable cycling is obtained for a graphite/LFP full-cell with an additive-free PC/EMC electrolyte (orange hexagonals), because PC does not form a stable SEI on graphite[54-58] and is therefore continuously reduced until all extractable Li^+ from LFP is consumed. The solvent co-intercalation in the graphite layers leads to exfoliation exposing fresh, unprotected graphite for further solvent reduction. This results in a first charge at a very low apparent cell voltage (2.6 V), without any discharge capacity after this first charge (see orange curve in Figure 4b). In contrast, all three additives (FEC, VC and CO_2) allow stable cycling in PC/EMC (Figure 4a). While the capacity and the capacity retention of the cells with 2% VC (red dots) are essentially identical to those of cells with the standard electrolyte EC/EMC (LP57, black squares), cells with 2% FEC (green diamonds) or CO_2 (blue triangles) have a much larger first cycle irreversible capacity (see Figure 4b) while their capacity fading is similar to that of the cell with VC or LP57. Please note that the irreversible capacity, i.e., the capacity drop between 1st and 2nd cycle, is relatively large for the here presented cells even with LP57 electrolyte. We correlate this behavior to the large specific surface area of the employed SLP30 graphite of 7 m^2/g, which necessitates an increased amount of SEI products for full protection of the active surface area, thereby consuming more Li-cations[56] and leading to a higher irreversible capacity. On the other hand, this
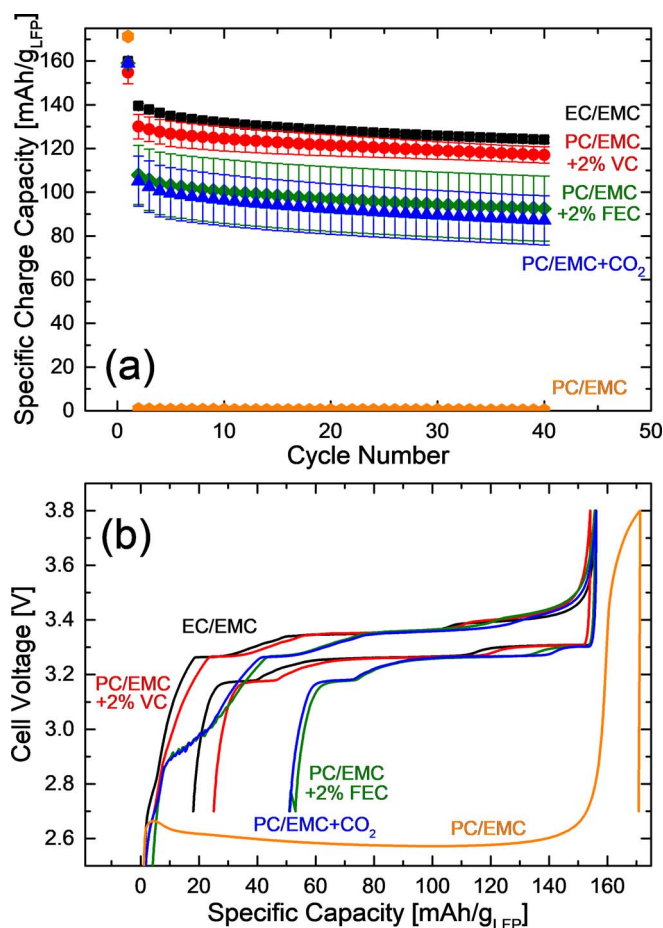
Figure 4. (a) Galvanostatic cycling performance (charge capacity) and (b) exemplary 1st cycle at C/20 of LFP/graphite electrodes in 1 M LiPF$_6$ in EC/EMC (3:7 w:w) or PC/EMC (3:7 w:w) without additives or with 2% of VC, 2% FEC, or under 1 atm CO$_2$. The cells were cycled between 3.8 V and 2.7 V at rates of C/20 (1st cycle), C/10 (2nd+3rd cycle) and C/5 (4th-40th cycle). The error bars represent the standard deviation of 3 repeat cells. Our in-house developed Li-air 1-compartment cell design was used to cycle the three cells with CO$_2$; for all other experiments two coin cells each were cycled in comparison to one cell with the Li-air-cell design, whereby no significant differences between the cell types were noted.

higher surface area facilitates better signals for spectroscopic and for gas analysis due to the increased amount of SEI products formed on the surface.

Regarding the voltage profiles in Figure 4b, the similarity between FEC (green curve) and CO$_2$ (blue curve) is striking. Due to a lower initial voltage plateau at the beginning of charge, during which irreversible processes take place, the first discharge capacity is lowered. Afterwards, stable cycling is possible with coulombic efficiencies almost as high as for LP57 and for PC/EMC+VC. The latter reacts according to the observed gas evolution (cf. Figure 3a) at a potential 500 mV higher than FEC, which might lead to an earlier passivation of the graphite and thus to less irreversible capacity losses in the first cycle. These observations confirm the work of Jeong et al.,[58] who cycled cells with FEC and VC in pure PC and also found higher stabilities for cells with VC.

Overall, it can be concluded that CO$_2$ is capable of forming a sufficiently protective SEI on graphite to allow stable cycling in a PC/EMC electrolyte, and CO$_2$ evolution during the initial additive reduction process may thus be an important part of an effective SEI forming additive like VC and FEC. Due to the more complicated handling of CO$_2$ in comparison to liquid additives, the early successful application of CO$_2$ in lithium-ion batteries[17–23] may have been forgotten over time.

OEMS analysis of carbon black electrodes with and without $^{13}CO_2$.—To better understand the CO$_2$ consumption process, we investigated the gas concentrations in cells filled with CO$_2$ during the first CV cycle by OEMS. Both EC and EMC do not form additional CO$_2$ upon reduction and were therefore chosen for this experiment. However, EMC presumably decomposes to lithium alkoxides,[29] which could chemically react with CO$_2$.[59] In contrast, lithium ethylene dicarbonate (LEDC), the major product of EC reduction, is not expected to react chemically with CO$_2$. To distinguish between gases originating from electrolyte reduction and products of CO$_2$ reduction, the respective cells were filled with isotopically labeled $^{13}CO_2$.

Figures 5a and 5b show the current profile (upper panels) and the gas evolution (lower panels) during a voltammetric scan at 0.1 mV/s of a C65 electrode from OCV (~3 V) to 0.1 V vs. Li$^+$/Li and back to 2.0 V vs. Li$^+$/Li in argon-filled cells with EC + 1 M LiPF$_6$ and EMC + 1 M LiPF$_6$ electrolyte, respectively. For the EC electrolyte (Figure 5a), a characteristic reduction peak can be observed around 0.6 V vs. Li$^+$/Li. The evolution of ethylene starts just below 1 V vs. Li$^+$/Li and rises steeply until it reaches a plateau of 17 μmol/m$^2_{BET}$ at the vertex potential. Between 0.8 and 0.1 V vs. Li$^+$/Li, minor amounts of CO and H$_2$ (~2 μmol/m$^2_{BET}$) are observed. Apart from these gases, CO$_2$ is evolved starting at 2 V vs. Li$^+$/Li, reaches a maximum of 1 μmol/m$^2_{BET}$ at 1.5 V vs. Li$^+$/Li, and drops back to zero below 1 V vs. Li$^+$/Li. The dominant evolution of ethylene can be attributed to the major reduction pathway of EC to ethylene and lithium ethylene dicarbonate (LEDC).[16,49,60,61] The evolution of CO$_2$ is presumably initiated by the reaction of OH$^-$, a product of trace water reduction and EC.[62,63] A reduction of CO$_2$ to CO seems unlikely here, as CO evolves only below 1 V vs. Li$^+$/Li, where CO$_2$ is already completely consumed. However, CO has been suggested as the product of a direct 2-electron reduction of EC.[64–66] The simultaneous evolution of H$_2$ could result from the reduction of residual H$_2$O,[62] protic impurities such as HF[47] or the direct reduction of EC.[61,67]

For an EMC + 1 M LiPF$_6$ electrolyte (Figure 5b), CO is the major evolved gas. Its evolution proceeds in two steps, with a lower rate during the first step between 1.5 and 0.6 V vs. Li$^+$/Li and a sharp increase between 0.6 and 0.1 V vs. Li$^+$/Li. Neither CO$_2$ nor H$_2$ were observed during the measurement, yet strong signals related to the ester exchange reaction of EMC to DMC and DEC were detected (not shown). Note that for this reason, the m/z = 12 trace was chosen for quantification of the CO signal, as the typically used m/z = 28 is superimposed by trans-esterification signals. A more detailed discussion of the reduction mechanism of EMC and the trans-esterification can be found in Strehle et al.[28]

Figures 5c and 5d show the corresponding EC and EMC model electrolytes in cells filled with a $^{13}CO_2$/Ar mixture. Both current profiles (upper panels) show a peak around 0.6 V vs. Li$^+$/Li. Between 1.5 V and 0.1 V vs. Li$^+$/Li, a total of ~70 μmol/m$^2_{BET}$ and ~65 μmol/m$^2_{BET}$ $^{13}CO_2$ is consumed in EC and EMC, respectively (middle panels). The rate plots (lower panels) show that in both electrolytes, the $^{13}CO_2$ consumption proceeds through 3 steps with their rate maxima at 1.5 V, 0.7 V, and 0.1 V vs. Li$^+$/Li. Interestingly, no ^{13}CO evolution is observed at any of these steps, clearly disproving the previous assumption that CO$_2$ could be reduced to CO and Li$_2$CO$_3$.[16,18] The additional H$_2$ evolution in both $^{13}CO_2$ cells is attributed to the different gas filling procedure, which unfortunately seems to introduce some trace moisture into these cells; this should, however, not affect the main finding, namely the consumption of CO$_2$ without CO evolution. In the cell with EC and $^{13}CO_2$, the ethylene evolution is further roughly halved, amounting to 7 μmol/m$^2_{BET}$, compared to the measurement in argon (Figure 5c). The CO evolution in the EMC cell with $^{13}CO_2$ (Figure 5d) is even more drastically reduced, yielding only 1/5 of the amount released in the same electrolyte in argon (Figure 5b). Additionally, we could not detect any OEMS signals related to the trans-esterification of EMC[28] in the EMC/$^{13}CO_2$ cell.

The striking similarity of the amount and pattern of the $^{13}CO_2$ consumption in EC and EMC suggests that its pathway is independent of the solvent, and hence proceeds as an electrochemical reduction reaction and not as a chemical reaction with solvent decomposition
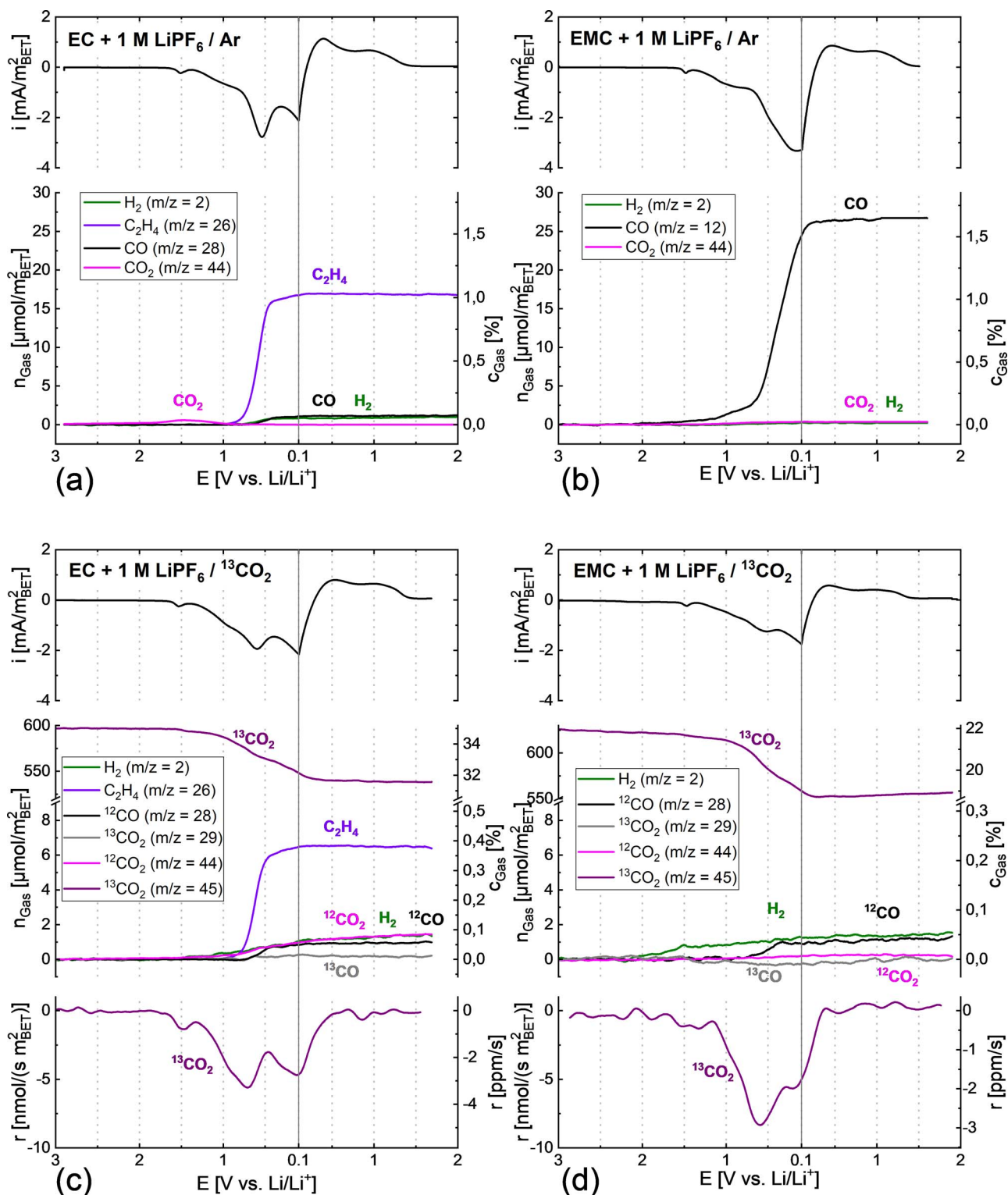
Figure 5. Gas evolution of a Super C65 carbon electrode during the first CV cycle at 0.1 mV/s using various model electrolytes with 1 M $LiPF_6$ in (a) EC, (b) EMC, (c) EC with $^{13}CO_2$ added to the cell head-space, or (d) EMC with added $^{13}CO_2$. The carbon working electrode is separated from the metallic lithium counter electrode with an aluminum sealed solid electrolyte diffusion barrier in the here used 2-compartment OEMS cell.

products. In both cases, the presence of CO_2 can effectively suppress the decomposition of the original solvent. The stronger CO_2 induced suppression of electrolyte decomposition for EMC compared to EC can be explained by their different reduction potentials: While the EC and CO_2 reduction occur in the same potential range (1–0.5 V vs. Li$^+$/Li), EMC is mainly reduced at lower potentials (< 0.5 V vs.

Li$^+$/Li), where CO_2 has already formed a passivating layer on the electrode. As discussed above, the absence of ^{13}CO further indicates that the commonly assumed reduction of CO_2 to Li_2CO_3 and CO does not take place. Although Li_2CO_3 is commonly observed in the SEI of electrodes cycled in CO_2,[20,22,23,68] a reduction to lithium oxalate[69,70] or lithium formate[71] is also possible in aprotic solvents. Therefore, we
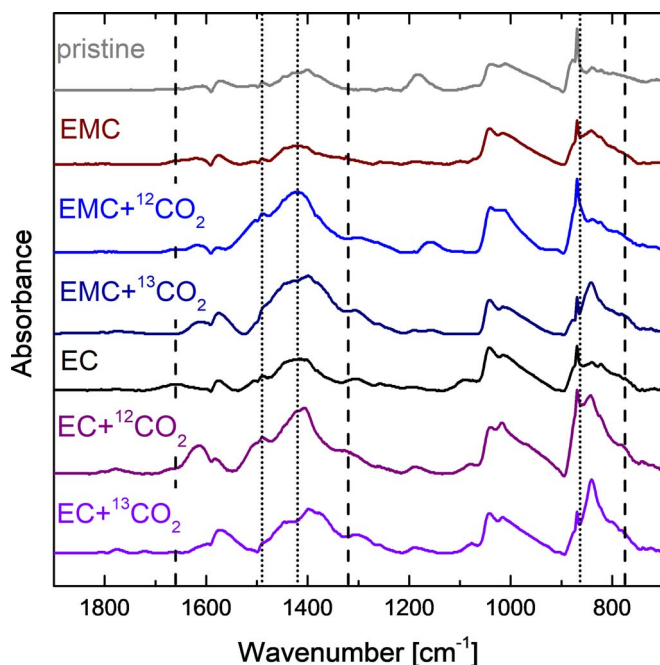
Figure 6. ATR-FTIR spectra of PVDF-bonded graphite electrodes after one formation cycle at C/20 between 2.7 and 3.9 V versus LFP in 1 M $LiPF_6$ in EC or EMC with and without CO_2. Both standard $^{12}CO_2$ and labeled $^{13}CO_2$ were added in order to investigate which SEI components contain the added CO_2. The spectrum nominated "pristine" consists of an unused graphite electrode. The dashed lines mark the band position for lithium oxalate, the dotted lines for lithium carbonate, assuming a standard salt containing ^{12}C.

take a closer look at the SEI components formed in the presence of CO_2.

FTIR analysis of electrodes after formation in CO₂.—In order to get a better understanding of the CO_2 consumption mechanism, FTIR spectra of graphite electrodes after one cycle at C/20 in an EMC or EC based electrolyte with and without CO_2 were analyzed. The cells were filled with both $^{12}CO_2$ and $^{13}CO_2$ to facilitate the assignment of the products formed due to CO_2 by the isotopic shift of the respective IR bands, the magnitude of which was estimated as follows.

The frequency ν of a vibrational band is determined by the coupling constant k and the reduced mass μ.

$$\nu = \frac{1}{2\pi}\sqrt{\frac{k}{\mu}} \quad \text{with} \quad \mu = \frac{m_1 m_2}{m_1 + m_2} \quad \text{for a two-atomic molecule}$$

$$[1]$$

Assuming that the coupling constant does not change due to an isotopic exchange, the shift of the frequency can be calculated as follows:

$$\nu_{Isotope} = \nu \sqrt{\frac{\mu}{\mu_{Isotope}}} \quad [2]$$

Even though these equations are only valid for molecules with two atoms, a rough estimation of the expected isotopic shift can be still calculated by considering a C and an O atom for vibrations from carbonates and carboxylates. The replacement of ^{12}C by ^{13}C would result in bands at a value of 97.8% of that of the original wavenumber.

Figure 6 shows the ATR-FTIR spectra of the graphite electrodes cycled in EMC and EC based electrolytes with and without CO_2. The spectra of the electrodes cycled in argon show mostly alkyl carbonates (vibrations around 1640 cm⁻¹, 1310 cm⁻¹, 1080 cm⁻¹ and 820 cm⁻¹) and are similar to the results by Nie et al. who analyzed binder-free electrodes in pure EC and EMC electrolytes.[49] The electrode cycled with $^{12}CO_2$ in EC contains additionally the characteristic asymmetric stretching vibration band of the CO_3^{2-} anion, which is largely increased

for the electrodes cycled in $^{12}CO_2$. The asymmetric stretching vibration is split in two due to the degeneration of the symmetry in Li_2CO_3, resulting in a band at 1490 cm⁻¹ and at 1420 cm⁻¹. These stretching vibration bands and the bending vibration band at 863 cm⁻¹ are marked by the dotted lines in Figure 6 and are clearly shifted for the electrodes cycled in EC+$^{13}CO_2$ within the wave number range expected for a ^{13}C replacement (i.e., for the stretching vibration bands by ca. 30 cm⁻¹). A similar shift is observed for the electrodes after the formation cycle in EMC+$^{13}CO_2$. However, the split stretching vibration band is less pronounced. Therefore, it is likely that it consists of a mixture of $Li_2^{12}CO_3$ and $Li_2^{13}CO_3$. This finding is surprising, as only very little $^{12}CO_3^{2-}$ (if any) was found on the electrode after formation in EMC and argon (cf. brown line in Figure 6). It suggests that due to the presence of CO_2, Li_2CO_3 is formed both directly from the CO_2 and the EMC molecule.

The dashed lines in Figure 6 mark the strongest vibrations of ^{12}C lithium oxalate. No clear bands are observed at these wavenumbers. However, there is also an isotopic shift of bands observed around 1600 cm⁻¹ when changing from $^{12}CO_2$ to $^{13}CO_2$. Unfortunately, these bands may belong to a variety of carbonates or carboxylates. In order to clarify the CO_2 reaction, we further applied NMR spectroscopy of D_2O extracts of cycled graphite electrodes to distinguish carboxylates like lithium formate or acetate from carbonates like lithium methyl or ethyl carbonate, which are unfortunately not clearly distinguishable by FTIR.

NMR analysis of electrodes after formation in CO₂.—Figure 7 displays exemplary ^1H and proton decoupled ^{13}C NMR spectra of D_2O extracts of graphite electrodes after one formation cycle in a pure EC or EMC based electrolyte. Before analyzing the spectra of the cells with CO_2 added to the gas-phase, the spectra of the argon flushed cells (black and brown line in Figure 7) are compared to a previous study by Nie et al.,[49] who analyzed binder free graphite electrodes in pure EMC and EC based electrolytes. Similar to Nie's study, we obtained for pure EC a strong singlet at 3.67 ppm in the ^1H spectrum, which can be related to LEDC formation on the electrode. For EMC the expected singlet of lithium methyl carbonate (LMC) at 3.36 ppm as well as a triplet at 1.19 ppm (J = 7.1 Hz) and a quartet at 3.65 ppm (J = 7.1 Hz), which can be related to lithium ethyl carbonate (LEC), were found by ^1H NMR.[49,72] For both electrolyte systems, a small amount of lithium acetate (LiAc) and lithium formate (LiForm) was detected and are marked in Figure 7a. Surprisingly, we found also some LEC and LMC in the EC cell, which cannot be explained by the commonly accepted EC decomposition mechanism[67] and which was not observed by Nie et al.[49] As expected, no LEDC was found in the EMC cell.

Regarding the ^{13}C NMR spectra in Figure 7b, only the main signals of LEC (16.7 and 57.3 ppm) and LMC (48.7 ppm) for EMC, as well as of LEDC (62.3 ppm) for EC were detected.[49,59] Furthermore, small signals at 167.8 ppm and 171.0 ppm, which can be related to Li_2CO_3 and lithium formate, were found. As no signal of the carbonate-C of LEDC, LMC or LEC is detectable, it is likely that the alkyl carbonates were quantitatively hydrolyzed by D_2O into alkoxides and Li_2CO_3.[73] This would further explain the detection of Li_2CO_3, which was only observed in traces by FTIR of the same electrodes from Ar-filled cells. The observed ^{13}C NMR signals may hence not directly belong to LEDC, LMC and LEC, but to ethylene glycolate, methoxide and ethoxide. Thus, a distinction between alkoxides and alkyl carbonates is unfortunately not feasible. Since alkoxides are commonly expected to be soluble in the electrolyte[74] and hence are not a major SEI product, we however believe that the NMR signals originate exclusively from the alkyl carbonates. Thus, the NMR signals are labeled as LEDC, LMC and LEC in the following. ^{19}F and ^{31}P NMR did not reveal any more insights, as only remaining trace amounts of $LiPF_6$ and LiF were found, in accordance to Nie et al.[49]

Figure 7a further shows the ^1H NMR spectra of cells after formation in a $^{13}CO_2$ enriched atmosphere. Surprisingly, no new products can be detected. However, the decomposition of EC and EMC is substantially reduced by the addition of CO_2, as the signals assigned to LEDC, LMC and LEC are decreased. In order to quantify this effect, TSP was added
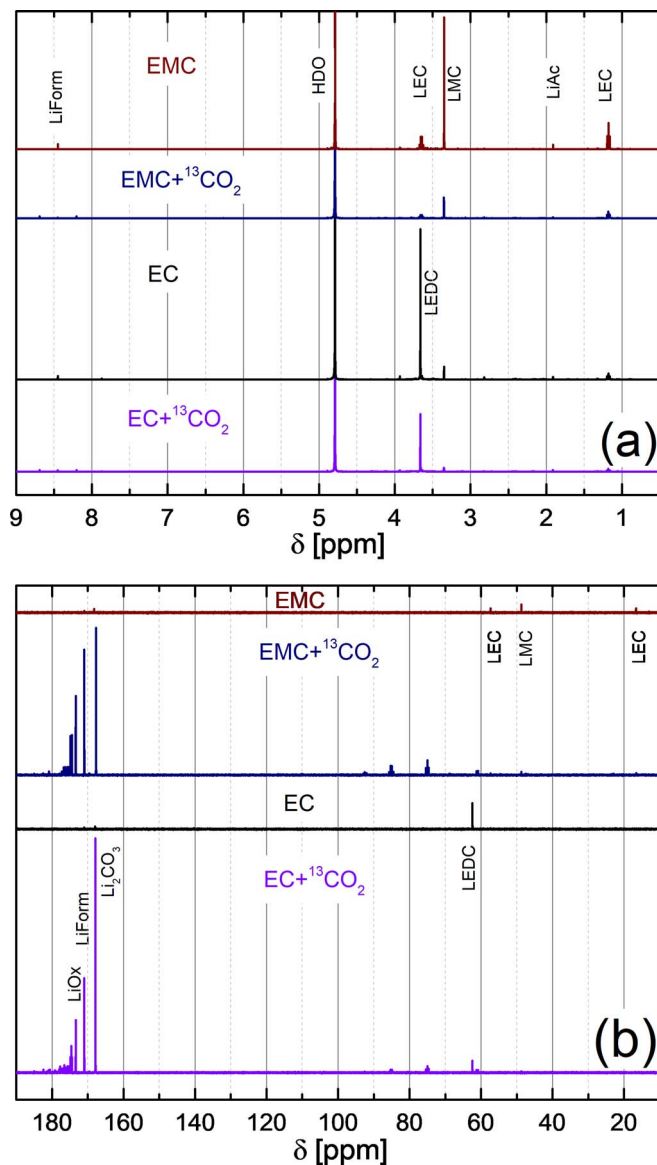
Figure 7. (a) ^{1}H and (b) ^{13}C NMR spectra of the D_2O extract of PVDF-bonded graphite electrodes after one formation cycle versus LFP in 1 M LiPF$_6$ in EC or EMC, with and without added CO_2 to the gas-phase. Both standard $^{12}CO_2$ and labeled $^{13}CO_2$ were added in order to investigate which SEI components contain the gas-phase CO_2. Note that here only the $^{13}CO_2$ labeled NMR data are shown. An enlarged version of the ^{13}C spectra in the 160–190 ppm region can be found in Figure S4.

Figure 8. SEI components in μmol/m$^2_{BET}$ quantified by ^{1}H NMR (LEC, LMC, LEDC, LiAc = lithium acetate, LiForm = lithium formate), by ^{13}C NMR (Li_2CO_3, $Li_2C_2O_4$) and by ^{19}F NMR (LiF) for graphite electrodes that have undergone formation in EC- or EMC-only electrolytes with or without added $^{13}CO_2$. Please note that Li_2CO_3 was only detected when originating from $^{13}CO_2$. Due to the hydrolysis of alkyl carbonates to alkoxides and Li_2CO_3, the amount of Li_2CO_3 cannot be quantified when no $^{13}CO_2$ for a distinction of the different origins is added. The raw data of this plot can be found in Tables S1 and S2.

to the NMR tubes and the molar concentration per electrode surface area is determined and given in Figure 8 and Table S1. It can be clearly seen that the amount of LEDC in the EC cells is approximately halved due to the addition of CO_2. This finding is in line with the results from the above OEMS analysis, where the addition of CO_2 also roughly halved the characteristic decomposition gas ethylene on the Super C65 electrode (cf. Figures 5a and 5c) as well as on the graphite electrodes (cf. Figure S1 and S2). The decomposition of EMC is even more suppressed, although the decrease of LMC and LEC in the SEI is less than the decrease of the evolved CO (cf. Figures 5b and 5d). This confirms that the formation mechanism of LMC and LEC is not directly connected to the evolution of CO, which is explained in detail in literature.[72,75] The suppression of solvent decomposition seems not to be related to the partial pressure of CO_2, as the amount of LEDC, LMC and LEC is roughly the same for a cell flushed with 1 atm $^{12}CO_2$ or a cell containing a $^{13}CO_2$/Ar mixture (cf. Table S1). Even though
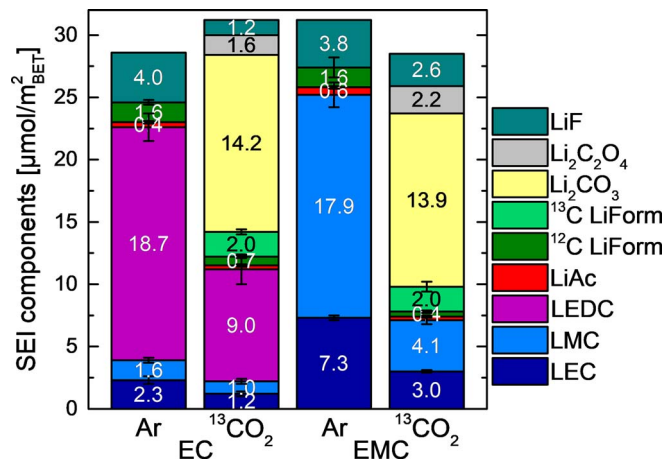
no new water-soluble products are observed due to the addition of CO_2, the incorporation of CO_2 is observed with ^{13}C labeled CO_2 due to ^{1}H-^{13}C coupling. The additional doublet at the position of lithium formate at 8.4 ppm with a coupling constant $^1J_{C-H}$ of 195 Hz[76] shows that $^{13}CO_2$ forms lithium formate. Furthermore, the lithium acetate signal at 1.9 ppm shows small amounts of a surrounding doublet with a coupling constant $^2J_{C-H}$ of 6 Hz. Even though $^{13}CO_2$ is hence clearly incorporated in the formed lithium acetate and lithium formate, the total amount of these species seems to be independent of whether CO_2 is added or not (cf. Table S1). In contrast, the lithium formate concentration seems to increase with the water concentration, as a larger lithium formate amount is found in cells filled with $^{13}CO_2$/Ar compared to $^{12}CO_2$. Due to the filling procedure and the lower dryness of $^{13}CO_2$ we assume a higher water content in those cells.

Figure 7b displays the ^{13}C NMR spectra of the argon flushed cells and the cells enriched with $^{13}CO_2$. In contrast to the ^{1}H NMR spectra, the signals belonging to products formed with $^{13}CO_2$ are clearly visible due to the signal enhancement by ^{13}C compared to products formed by non ^{13}C enriched species with a ^{13}C content of only 1.1%. The signals correlated to LEDC, LEC and LMC are diminished in accordance to the ^{1}H NMR spectra, while strong signals arise around 170 ppm which hence must be related to products formed with $^{13}CO_2$. With the help of reference samples, the signals at 167.7 ppm, 171.0 ppm and 173.4 ppm were identified as Li_2CO_3, lithium formate and lithium oxalate ($Li_2C_2O_4$), respectively. The signal of lithium formate was further confirmed by the coupling constant $^1J_{C-H}$ of 195 Hz in the spectrum without proton decoupling, matching the one in the ^{1}H NMR spectrum. A signal belonging to lithium acetate, which should appear around 181 ppm with a coupling constant of 6 Hz, was, however, not found. Several further signals between 174 and 178 ppm must also belong to carboxylates and carbonates, but could not be identified (cf. Figure S4 for magnification). The same is true for a triplet at 75 ppm and a quartet at 85 ppm in the proton decoupled spectrum with coupling constants of 53 and 51 Hz, typical for $^1J_{C-C}$.[76] This implies that the coupling must occur between ^{13}C labeled nuclei, indicating a more complex structure formed by several $^{13}CO_2$ units. The triplet forms an additional doublet ($^1J_{C-H}$ = 150 Hz) in the spectrum without proton decoupling, indicating a tertiary carbon in the unknown substance.

However, as these signals are rather small, we focus in the following on the three main products observed in the cells filled with $^{13}CO_2$, namely Li_2CO_3, lithium formate and lithium oxalate. In or-

der to quantify the signals, ^{13}C NMR spectra with a 25x prolonged relaxation delay were recorded to allow the full relaxation of the slowly relaxing carbonate nuclei. The surface normalized amounts obtained by referencing to the internal TSP standard are given in Table S2. For comparison with the quantification results from the ^{1}H NMR, the signal of LEDC from the graphite electrode in the $^{13}CO_2$/EC cell was also quantified assuming 1.1% of ^{13}C, as $^{13}CO_2$ cannot be incorporated in the CH_2-units of LEDC. 10 $\mu mol/m^2_{BET}$ LEDC were found in ^{13}C NMR of the $^{13}CO_2$/EC graphite electrode compared to 9 $\mu mol/m^2_{BET}$ by ^{1}H NMR. This difference is probably related to the sample preparation (addition of the standard). A slightly higher concentration was also determined for lithium formate by ^{13}C NMR in comparison to ^{1}H NMR in both EC-and EMC-based cells filled with $^{13}CO_2$, but the accuracy is reliable enough to quantify the amount of lithium oxalate in comparison to Li_2CO_3. Interestingly, the product distribution for EC and EMC with $^{13}CO_2$ is similar. While lithium oxalate occurs only in small amounts, roughly half of the amount of lithium formate, Li_2CO_3 is clearly the main product, in accordance to the FTIR spectra (cf. Figure 6). It should be, however, mentioned that due to the hydrolysis of alkyl carbonates by D_2O some Li_2CO_3 may arise from alkyl carbonates formed in the reaction of alkoxides and $^{13}CO_2$. This reaction was suggested to be responsible for the alkoxide scavenging effect of CO_2 stopping the trans-esterification of linear alkyl carbonate solvents.[28] The small amount of superposing $Li_2^{12}CO_3$ can, however, be neglected.

In order to quantify all the detected NMR products, we finally added C_6F_6 to the D_2O extracts of the electrodes to estimate the amount of LiF in the SEI, which is given in Figure 8 and Table S1. Similar to VC and FEC, the addition of CO_2 suppresses the $LiPF_6$ decomposition, as also less LiF was found in the electrodes of the CO_2 cells.

Discussion

SEI thickness.—In order to check whether the thickness of the SEI composed of the products found is reasonable, we estimated the number of monolayers derived from the surface normalized amounts obtained by NMR and summarized the results in Table S3. For this, we assumed that each atom of the found molecules occupies a square with an edge length of a carbon-carbon single bond (0.15 nm).[77] The resulting 2.7 to 5 monolayers seem reasonable. The actual SEI thickness might be higher, as some products may not adsorb flat on the surface, and as products insoluble in D_2O such as polymers are not taken into account. Nevertheless, it appears that the total amount of SEI monolayers is decreased due to the addition of CO_2. This might mean that the main product of CO_2, namely Li_2CO_3, passivates the graphite anode more efficiently than a bulkier alkyl carbonate which may not lie completely flat on the surface. It should, however, also be mentioned that the SEI is thicker in a pure EC cell than in a pure EMC cell. This correlates with the observation from the XPS spectra (cf. Figure 2b), where the graphite peak could be seen in the spectra from electrodes in EMC electrolyte but not for electrodes cycled in EC. As the passivation properties of EC are superior compared to EMC,[78] it is difficult to judge whether a thinner or a thicker SEI is at the end advantageous.

The formation of Li_2CO_3.—The FTIR and NMR analyses show clear evidence that Li_2CO_3 is the major product due to intentionally added CO_2 on the graphite electrode in Li-ion battery cells. However, no CO was detected by OEMS upon the consumption of CO_2, which clearly excludes the previously hypothesized mechanism:[18]

$$2\,CO_2 + 2\,e^- + 2\,Li^+ \rightarrow CO + Li_2CO_3 \qquad [3]$$
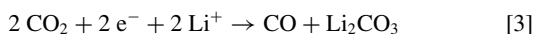
A fraction of the detected Li_2CO_3 can be explained by the reduction of trace water and its subsequent reaction with CO_2:

$$H_2O + e^- \rightarrow 0.5\,H_2 + OH^- \qquad [4]$$

$$CO_2 + OH^- + 2\,Li^+ \rightarrow Li_2CO_3 + H^+ \qquad [5]$$
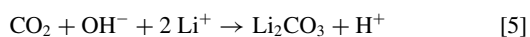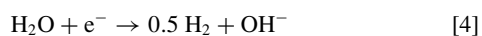
Reactions 4 and 5 explain further the effect that more water leads to more Li_2CO_3 and less LEDC in the SEI.[79] Water is expected to be reduced at approximately 1.5 V vs. Li$^+$/Li.[62,80] As can be seen in Figures 5a–5d, a clear reduction peak can be observed in the voltage profile at this potential. The integration of this peak yields an electric charge which would be required to reduce approximately 40–50 ppm of water. Summing the trace water contained in the electrolyte (a minor amount, as water converts to HF during storage),[47] in the electrodes and introduced by the gas filling procedure, this amount seems reasonable. At this potential, the first (minor) CO_2 consumption process takes place (see Figures 5c and 5d), in agreement with Reaction 5. Surprisingly, no hydrogen is evolved at this potential in argon-filled cells (Figures 5a and 5b), although hydrogen evolution can be observed in cells filled with $^{13}CO_2$ (Figures 5c and 5d), which probably contain more moisture due to the $^{13}CO_2$ filling procedure.

The main consumption of CO_2 takes place in a second process around 0.7 V vs. Li$^+$/Li (see Figures 5c and 5d), which fits to the suggestion that the reduction of CO_2 to $CO_2^{\bullet-}$ radicals occurs at lower potentials than the water reduction:[81]

$$CO_2 + e^- \rightarrow CO_2^{\bullet-} \qquad [6]$$
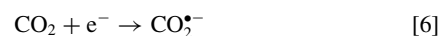
$CO_2^{\bullet-}$ radicals will recombine forming lithium oxalate:

$$2\,CO_2^{\bullet-} + 2\,Li^+ \rightarrow Li_2C_2O_4 \qquad [7]$$
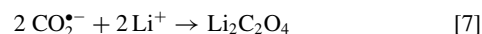
Furthermore, $CO_2^{\bullet-}$ radicals can react in the presence of protons produced by Reaction 5 or other protic impurities, e.g. from HF, to lithium formate:

$$CO_2^{\bullet-} + H^+ + Li^+ + e^- \rightarrow HCO_2Li \qquad [8]$$
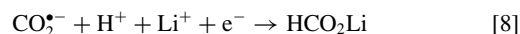
In order to produce the 1.6–3.3 $\mu mol/m^2_{BET}$ of lithium formate detected (cf. Figure 8 as well as Table S1 and S2), about 15–40 ppm of protons in the form of water or HF are needed in the electrolyte. Assuming that water is the only protic impurity and that according to Reactions 4 and 5 one proton would be released into the electrolyte per water molecule, the formed amount of lithium formate is comparable to the amount of water determined by the charge flowing at the water reduction potential of 1.5 V vs. Li$^+$/Li in the voltage profile. As the amount of water is much smaller than the amount of CO_2 in CO_2-filled cells, it makes sense that the amount of lithium formate scales with the water content (cells filled with $^{13}CO_2$ are suspected to contain more moisture than cells with $^{12}CO_2$ or argon) but not directly with CO_2 as can be seen in Figure 8 and Table S1.

If Reactions 4 and 5 were the only occurring processes leading to Li_2CO_3, the ratio of Li_2CO_3:H_2O should be 1:1. However, only around 5 $\mu mol/m^2_{BET}$ Li_2CO_3 of the 14 $\mu mol/m^2_{BET}$ found (cf. Table S2) can be explained by these reactions assuming 40–50 ppm of water. Another possible mechanism for the detection of a substantial amount of Li_2CO_3 by NMR may stem from the Dumas-Peligot reaction,[82] which is utilized to synthesize alkyl carbonates.[59,73,83–85] Alkoxides formed during solvent decomposition[72] react with CO_2 to the corresponding alkyl carbonates, but are hydrolized in D_2O and only the ^{13}C labeled Li_2CO_3 is detected. However, since Li_2CO_3 is also the main product in the FTIR spectra (cf. Figure 6), where any contact of the electrodes with water was carefully avoided, this reaction cannot be responsible for the main share of Li_2CO_3 formed, unless alkyl carbonates can be further reduced to Li_2CO_3. Yet, this seems not very likely, as alkyl carbonates are a major part of the SEI (cf. Figure 8 as well as Table S1 and S3) and only little Li_2CO_3 is found in the absence of CO_2. Furthermore, alkoxides are a major decomposition product of linear, but not of cyclic alkyl carbonates, as can be seen by the significant lower amount of CO evolved from EC reduction compared to EMC reduction (see Figures 5a and 5b). Therefore, the similar product distribution for the EMC and the EC cell would be hard to explain with this mechanism. In order to prove that CO is simply just not detected by OEMS due to some consecutive reactions with carbonate electrolyte decomposition products, the gas evolution of a cell with 0.5 M LiTFSI in diglyme as electrolyte and added $^{13}CO_2$ was monitored. Figure 9 indicates a $^{13}CO_2$ consumption in this cell of approximately 110 $\mu mol/m^2_{BET}$, which is
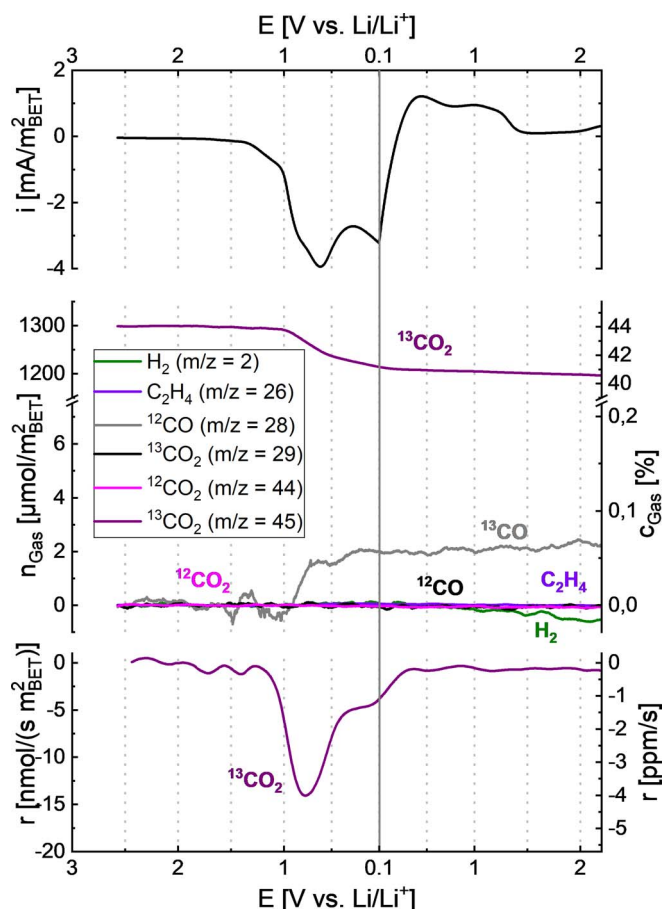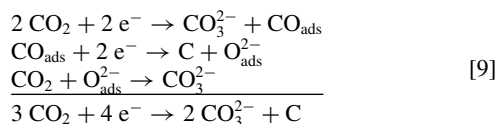
Figure 9. Gas evolution of a Super C65 carbon electrode during one CV cycle at 0.1 mV/s in the model electrolyte 0.5 M LiTFSI in diglyme with $^{13}CO_2$ added to the gas-phase. The carbon working electrode is separated from the metallic lithium counter electrode with an aluminum sealed solid electrolyte diffusion barrier in the here used 2-compartment OEMS cell.

higher compared to the cells with carbonate-based electrolytes (65–70 $\mu mol/m_{BET}^2$, see Figures 5c and 5d). In contrast to the carbonate electrolytes, a small amount of 2 $\mu mol/m_{BET}^2$ ^{13}CO was detected. However, the amount of ^{13}CO detected in the diglyme electrolyte is by far too low to explain the CO_2 consumption via Reaction 3.

Zhuang et al.[86] suggested that CO is not evolved due to its further reduction to carbon according to the following mechanism, which would lead to additional Li_2CO_3:

$$\begin{array}{c} 2\,CO_2 + 2\,e^- \rightarrow CO_3^{2-} + CO_{ads} \\ CO_{ads} + 2\,e^- \rightarrow C + O_{ads}^{2-} \\ \underline{CO_2 + O_{ads}^{2-} \rightarrow CO_3^{2-}} \\ \hline 3\,CO_2 + 4\,e^- \rightarrow 2\,CO_3^{2-} + C \end{array} \qquad [9]$$

A similar mechanism is also claimed for the reduction of CO_2 in Li-CO_2 batteries,[87–90] where the formation of amorphous carbon was confirmed by Liu et al.[88] and Qiao et al.[90] Since 5 $\mu mol/m_{BET}^2$ of the Li_2CO_3 detected by NMR (cf. Figure 8 and Table S2) can be explained by Reactions 4 and 5, 9 $\mu mol/m_{BET}^2$ (viz., 14 $\mu mol/m_{BET}^2$ - 5 $\mu mol/m_{BET}^2$) must be explained differently. In case that all of the remaining 9 $\mu mol/m_{BET}^2$ Li_2CO_3 is formed according to Reaction 9, 4.5 $\mu mol/m_{BET}^2$ of amorphous carbon should be additionally formed from the consumed CO_2.

The consumption of CO_2 is, as can be seen in the gas evolution rate of Figures 5b and 5d, not continuous, but composed of three different processes. The first one at 1.5 V vs. Li$^+$/Li is related to the reduction of water and formation of Li_2CO_3 (cf. Reactions 4 and 5). The second one at 0.7 V vs. Li$^+$/Li belongs to the CO_2 reduction to

$CO_2^{\bullet-}$ (cf. Reaction 6) and subsequent formation of lithium oxalate and lithium formate according to Reactions 7 and 8. The third CO_2 consumption process around 0.1 V vs. Li$^+$/Li may hence be explained by further CO_2 reduction according to Reaction 9, as (almost) no CO was detected by OEMS.

Reactions 4 to 9 give a plausible explanation for the detected amount of Li_2CO_3, lithium formate and lithium oxalate by ^{13}C NMR (cf. Table S2). However, the total CO_2 consumption observed in the OEMS measurements does not very well match the amount of products found by NMR. The cell with EC and $^{13}CO_2$ consumed ∼58 $\mu mol/m_{BET}^2$ CO_2 (Figure 5c), the cell with EMC and $^{13}CO_2$ ∼72 $\mu mol/m_{BET}^2$ CO_2 (Figure 5d). The difference between EC and EMC might be related to the above mentioned reaction of alkoxides and CO_2, which should occur in particular for linear carbonates. Still, less than 25 $\mu mol/m_{BET}^2$ of $^{13}CO_2$ was consumed for the products detected in the ^{13}C NMR spectra (cf. Table S2). This mismatch may be related to the two different cell set-ups used: while the OEMS measurements were performed with a 2-compartment half-cell and carbon black electrodes, the NMR analysis was done with LFP-graphite full-cells. To clarify whether this may lead to different SEI compositions, we performed an additional OEMS measurement of a graphite electrode with an EC electrolyte and $^{13}CO_2$ in a 2-compartment cell, and indeed only 36 $\mu mol/m_{BET}^2$ of CO_2 was consumed (see Figure S2). A similar experiment with argon-filled cells revealed that also the ethylene reduction per m_{BET}^2 is about 1.7 times higher for the C65 carbon black compared to SLP30 graphite (see Figure S1), which is probably related to the different surface structure of edge and basal planes of the graphite. We further hypothesize that the lower consumption of CO_2 with graphite is related to the ≈10x smaller surface area of SLP30 compared to C65, while the amount of trace water in the electrolyte is the same, leading to a more immediate surface passivation by water reduction and Li_2CO_3 formation (see Reactions 4 and 5) and to less CO_2 consumption by subsequent processes on the low-surface area graphite electrodes. An OEMS measurement of a galvanostatically cycled full-cell with an SLP30 graphite anode and LFP as counter electrode instead of lithium, led to a similar CO_2 consumption of 32 $\mu mol/m_{BET}^2$ (see Figure S3). Hence, using LFP in a 1-compartment cell instead of the 2-compartment cell with lithium counter electrode does not influence the measurement as much as using C65 carbon instead of graphite. Comparing the products found by NMR (< 25 $\mu mol/m_{BET}^2$) and the CO_2 consumed by OEMS (32 $\mu mol/m_{BET}^2$) in the same cell configuration, leaves a gap of only 7 $\mu mol/m_{BET}^2$. 4.5 $\mu mol/m_{BET}^2$ of the missing 7 $\mu mol/m_{BET}^2$ can be explained with the amorphous carbon formed according to Reaction 9, which cannot be detected in the D_2O extract by NMR. Furthermore, small amounts of products may not be detected by NMR, because they might be insoluble in D_2O such as polymers. Substantial losses due to the rinsing of the electrodes can, however, be excluded as a non-washed electrode cycled in EMC under a CO_2 atmosphere showed similar results to the rinsed equivalent.

Conclusions

In this paper the effect of the two most common SEI forming additives VC and FEC were directly compared on carbonaceous electrodes. The decomposition of both additives leads to a polymeric carbonate. While VC suppresses the formation of LiF, FEC increases the amount of LiF in the electrode. CO_2 is next to trace amounts of CO the only gaseous decomposition product during formation for both additives.

Interestingly, the addition of CO_2 to LFP/graphite cells with PC/EMC electrolyte allowed stable cycling, very similar to cells with 2% FEC in PC/EMC, while cells without additives in a PC/EMC electrolyte could not be discharged even once. Mass spectrometric analysis of the gas evolution during formation of cells filled with gaseous CO_2 revealed that in contrast of common beliefs, no CO is evolved due to the reduction of CO_2, even though Li_2CO_3 was found to be the main additional compound of the SEI in the presence of gaseous CO_2. Furthermore, lithium formate and lithium oxalate were detected for cells with both pure EC and pure EMC electrolyte filled with CO_2. Quantification with NMR demonstrated that the concentration of lithium

carbonate, formate and oxalate is comparable for cells with EC and EMC, suggesting a CO_2 reaction mechanism independent of the decomposition pathway of the used solvent. CO_2 led further to a clear suppression of typical solvent decomposition products.

Hence, we conclude that the addition of CO_2 or CO_2-evolving additives are clearly beneficial for the formation of the SEI. CO_2 leads in combination with water and HF to a first passivation layer made of lithium formate and carbonate at potentials starting around 1.5 V vs. Li^+/Li, which suppresses the later decomposition of the solvents once potentials are reached. We believe therefore that CO_2 in combination with trace water is advantageous for the initial formation of the SEI.

ORCID

K. Uta Schwenke https://orcid.org/0000-0003-1798-3894
Sophie Solchenbach https://orcid.org/0000-0001-6517-8094
Brett L. Lucht https://orcid.org/0000-0002-4660-0840

References

1. E. Peled, *J. Electrochem. Soc.*, **126**, 2047 (1979).
2. M. Nie, J. Demeaux, B. T. Young, D. R. Heskett, Y. Chen, A. Bose, J. C. Woicik, and B. L. Lucht, *J. Electrochem. Soc.*, **162**, A7008 (2015).
3. H. Nakai, T. Kubota, A. Kita, and A. Kawashima, *J. Electrochem. Soc.*, **158**, A798 (2011).
4. V. Etacheri, O. Haik, Y. Goffer, G. A. Roberts, I. C. Stefan, R. Fasching, and D. Aurbach, *Langmuir*, **28**, 965 (2012).
5. M. Nie, D. P. Abraham, Y. Chen, A. Bose, and B. L. Lucht, *J. Phys. Chem. C*, **117**, 13403 (2013).
6. E. Markevich, K. Fridman, R. Sharabi, R. Elazari, G. Salitra, H. E. Gottlieb, G. Gershinsky, A. Garsuch, G. Semrau, M. A. Schmidt et al., *J. Electrochem. Soc.*, **160**, A1824 (2013).
7. I. A. Profatilova, C. Stock, A. Schmitz, S. Passerini, and M. Winter, *J. Power Sources*, **222**, 140 (2013).
8. C. C. Nguyen and B. L. Lucht, *J. Electrochem. Soc.*, **161**, A1933 (2014).
9. H. Ota, Y. Sakata, A. Inoue, and S. Yamaguchi, *J. Electrochem. Soc.*, **151**, A1659 (2004).
10. B. Zhang, M. Metzger, S. Solchenbach, M. Payne, S. Meini, H. A. Gasteiger, A. Garsuch, and B. L. Lucht, *J. Phys. Chem. C*, 150512180451000 (2015).
11. A. L. Michan, B. S. Parimalam, M. Leskes, R. N. Kerber, T. Yoon, C. P. Grey, and B. L. Lucht, *Chem. Mater.*, **28**, 8149 (2016).
12. I. A. Profatilova, S.-S. Kim, and N.-S. Choi, *Electrochim. Acta*, **54**, 4445 (2009).
13. H. Ota, K. Shima, M. Ue, and J. Yamaki, *Electrochim. Acta*, **49**, 565 (2004).
14. R. Jung, M. Metzger, D. Haering, S. Solchenbach, C. Marino, N. Tsiouvaras, C. Stinner, and H. A. Gasteiger, *J. Electrochem. Soc.*, **163**, A1705 (2016).
15. M. E. Spahr, T. Palladino, H. Wilhelm, A. Würsig, D. Goers, H. Buqa, M. Holzapfel, and P. Novák, *J. Electrochem. Soc.*, **151**, A1383 (2004).
16. D. Aurbach, Y. Gofer, M. Ben-Zion, and P. Aped, *J. Electroanal. Chem.*, **339**, 451 (1992).
17. J. O. Besenhard, M. W. Wagner, M. Winter, A. D. Jannakoudakis, P. D. Jannakoudakis, and E. Theodoridou, *J. Power Sources*, **44**, 413 (1993).
18. D. Aurbach and O. Chusid, *Electrochem. Soc. Lett.*, **140**, 194 (1993).
19. O. Youngman Chusid, E. Ein Ely, D. Aurbach, M. Babai, and Y. Carmeli, *J. Power Sources*, **43**, 47 (1993).
20. D. Aurbach, Y. Ein-Eli, O. Chusid, Y. Carmeli, M. Babai, and H. Yamin, *J. Electrochem. Soc.*, **141**, 603 (1994).
21. D. Aurbach, Y. Ein-Ely, and A. Zaban, *J. Electrochem. Soc.*, **141**, L1 (1994).
22. Y. Ein-Eli, B. Markovsky, D. Aurbach, Y. Carmeli, H. Yamin, and S. Luski, *Electrochim. Acta*, **39**, 2559 (1994).
23. D. Aurbach, Y. Ein-Eli, B. Markovsky, A. Zaban, S. Luski, Y. Carmeli, and H. Yamin, *J. Electrochem. Soc.*, **142**, 2882 (1995).
24. T. Osaka, T. Momma, T. Tajima, and Y. Matsumoto, *J. Electrochem. Soc.*, **142**, 1057 (1995).
25. D. Aurbach and Y. S. Cohen, *J. Electrochem. Soc.*, **144**, 3355 (1997).
26. L. J. Krause, V. L. Chevrier, L. D. Jensen, and T. Brandt, *J. Electrochem. Soc.*, **164**, A2527 (2017).
27. S. Solchenbach, M. Wetjen, D. Pritzl, K. U. Schwenke, and H. A. Gasteiger, *J. Electrochem. Soc.*, **165**, A512 (2018).
28. B. Strehle, S. Solchenbach, M. Metzger, K. U. Schwenke, and H. A. Gasteiger, *J. Electrochem. Soc.*, **164**, A2513 (2017).
29. E. S. Takeuchi, H. Gan, M. Palazzo, R. A. Leising, and S. M. Davis, *J. Electrochem. Soc.*, **144**, 1944 (1997).
30. S. Meini, M. Piana, N. Tsiouvaras, A. Garsuch, and H. A. Gasteiger, *Electrochem. Solid-State Lett.*, **15**, A45 (2012).
31. N. Tsiouvaras, S. Meini, I. Buchberger, and H. A. Gasteiger, *J. Electrochem. Soc.*, **160**, A471 (2013).
32. M. Metzger, C. Marino, J. Sicklinger, D. Haering, and H. A. Gasteiger, *J. Electrochem. Soc.*, **162**, A1123 (2015).
33. M. Metzger, B. Strehle, S. Solchenbach, and H. A. Gasteiger, *J. Electrochem. Soc.*, **163**, A798 (2016).
34. J. M. Martinez del la Hoz and P. B. Balbuena, *Phys. Chem. Chem. Phys.*, **16**, 17091 (2014).
35. D. Y. Wang, N. N. Sinha, J. C. Burns, C. P. Aiken, R. Petibon, and J. R. Dahn, *J. Electrochem. Soc.*, **161**, 467 (2014).
36. D. Pritzl, S. Solchenbach, M. Wetjen, and H. A. Gasteiger, *J. Electrochem. Soc.*, **164**, A2625 (2017).
37. R. Petibon, J. Xia, J. C. Burns, and J. R. Dahn, *J. Electrochem. Soc.*, **161**, A1618 (2014).
38. R. Petibon, V. L. Chevrier, C. P. Aiken, D. S. Hall, S. R. Hyatt, R. Shunmugasundaram, and J. R. Dahn, *J. Electrochem. Soc.*, **163**, A1146 (2016).
39. D. Aurbach, K. Gamolsky, B. Markovsky, Y. Gofer, M. A. Schmidt, and U. Heider, *Electrochim. Acta*, **47**, 1423 (2002).
40. L. El Ouatani, R. Dedryvère, C. Siret, P. Biensan, S. Reynaud, P. Iratçabal, and D. Gonbeau, *J. Electrochem. Soc.*, **156**, A103 (2009).
41. I. A. Profatilova, N.-S. Choi, S. W. Roh, and S.-S. Kim, *J. Power Sources*, **192**, 636 (2009).
42. C. Xu, F. Lindgren, B. Philippe, M. Gorgoi, F. Björefors, K. Edström, and T. Gustafsson, *Chem. Mater.*, **27**, 2591 (2015).
43. K. W. Schroder, J. Alvarado, T. A. Yersak, J. Li, N. J. Dudney, L. J. Webb, Y. S. Meng, and K. J. Stevenson, *Chem. Mater.*, **27**, 5531 (2015).
44. S. Dalavi, P. R. Guduru, and B. L. Lucht, *J. Electrochem. Soc.*, **159**, A642 (2012).
45. J. Jones, M. Anouti, M. Caillon-Caravanier, P. Willmann, P. Y. Sizaret, and D. Lemordant, *Fluid Phase Equilib.*, **305**, 121 (2011).
46. M. Nie and B. L. Lucht, *J. Electrochem. Soc.*, **161**, A1001 (2014).
47. D. Strmcnik, I. E. Castelli, J. G. Connell, D. Haering, M. Zorko, P. Martins, P. P. Lopes, B. Genorio, T. Østergaard, H. A. Gasteiger et al., *Nat. Catal.*, **1**, 255 (2018).
48. L. El Ouatani, R. Dedryvère, C. Siret, P. Biensan, and D. Gonbeau, *J. Electrochem. Soc.*, **156**, A468 (2009).
49. M. Nie, D. Chalasani, D. P. Abraham, Y. Chen, A. Bose, and B. L. Lucht, *J. Phys. Chem. C*, **117**, 1257 (2013).
50. I. A. Shkrob, J. F. Wishart, and D. P. Abraham, *J. Phys. Chem. C*, **119**, 14954 (2015).
51. F. A. Soto, Y. Ma, J. M. Martinez del la Hoz, J. M. Seminario, and P. B. Balbuena, *Chem. Mater.*, acs.chemmater.5b03358 (2015).
52. K. Ushirogata, K. Sodeyama, Y. Okuno, and Y. Tateyama, *J. Am. Chem. Soc.*, **1335**, 11967 (2013).
53. Y. Okuno, K. Ushirogata, K. Sodeyama, and Y. Tateyama, *Phys. Chem. Chem. Phys.*, **18**, 8643 (2016).
54. J. O. Besenhard and H. P. Fritz, *Electroanal. Chem. Interfacial Electrochem.*, **53**, 329 (1974).
55. A. N. Dey and B. P. Sullivan, *J. Electrochem. Soc.*, **117**, 222 (1970).
56. R. Fong, U. von Sacken, and J. R. Dahn, *J. Electrochem. Soc.*, **137**, 2009 (1990).
57. K. Xu, *J. Electrochem. Soc.*, **156**, A751 (2009).
58. S. Jeong, M. Inaba, R. Mogi, Y. Iriyama, and A. Abouimrane, *Langmuir*, **17**, 8281 (2001).
59. L. Gireaud, S. Grugeon, S. Laruelle, S. Pilard, and J.-M. Tarascon, *J. Electrochem. Soc.*, **152**, A850 (2005).
60. G. V. Zhuang, K. Xu, H. Yang, T. R. Jow, and P. N. Ross, *J. Phys. Chem. B*, **109**, 17567 (2005).
61. R. Imhof and P. Novák, *J. Electrochem. Soc.*, **145**, 3313 (1998).
62. R. Bernhard, M. Metzger, and H. A. Gasteiger, *J. Electrochem. Soc.*, **162**, A1984 (2015).
63. M. Metzger, B. Strehle, S. Solchenbach, and H. A. Gasteiger, *J. Electrochem. Soc.*, **163**, A1219 (2016).
64. R. Mogi, M. Inaba, Y. Iriyama, T. Abe, and Z. Ogumi, *J. Power Sources*, **119–121**, 597 (2003).
65. M. Onuki, S. Kinoshita, Y. Sakata, M. Yanagidate, Y. Otake, M. Ue, and M. Deguchi, *J. Electrochem. Soc.*, **155**, A794 (2008).
66. K. Leung, *Chem. Phys. Lett.*, **568–569**, 1 (2013).
67. M. Winter, R. Imhof, F. Joho, and P. Novák, *J. Power Sources*, **81–82**, 818 (1999).
68. D. Aurbach, B. Markovsky, I. Weissman, E. Levi, and Y. Ein-Eli, *Electrochim. Acta*, **45**, 67 (1999).
69. C. Amatore and J.-M. Saveant, *J. Am. Chem. Soc.*, **103**, 5021 (1981).
70. V. U. Kaiser and E. Heitz, *Berichte der Bunsen-Gesellschaft*, **10**, 818 (1973).
71. L. V Haynes and D. T. Sawyer, *Anal. Chem.*, **39**, 332 (1958).
72. T. Sasaki, A. Abouimrane, Y. Iriyama, M. Inaba, and Z. Ogumi, *J. Power Sources*, **150**, 208 (2005).
73. K. Xu, G. V. Zhuang, J. L. Allen, U. Lee, S. S. Zhang, P. N. Ross, and T. R. Jow, *J. Phys. Chem. B*, **110**, 7708 (2006).
74. G. Gachot, S. Grugeon, M. Armand, S. Pilard, P. Guenot, J.-M. Tarascon, and S. Laruelle, *J. Power Sources*, **178**, 409 (2008).
75. H. Yoshida, T. Fukunaga, T. Hazama, M. Terasaki, M. Mizutani, and M. Yamachi, *J. Power Sources*, **68**, 311 (1997).
76. J. B. Lambert and E. P. Mazzola, *Nuclear Magnetic Resonance Spectroscopy*, Pearson Education Inc., (2004).
77. D. R. Lide, *Tetrahedron*, **17**, 125 (1962).

78. Y. Ein-Eli, S. R. Thomas, and V. R. Koch, *J. Electrochem. Soc.*, **143**, L273 (1996).
79. K. Edström, M. Herstedt, and D. P. Abraham, *J. Power Sources*, **153**, 380 (2006).
80. Y. E. Ely and D. Aurbach, *Langmuir*, **8**, 1845 (1992).
81. P. A. Christensen, A. Hamnett, A. V. G. Muir, and N. A. Freeman, *J. Electroanal. Chem.*, **288**, 197 (1990).
82. J. Dumas and E. Peligot, *Justus Liebigs Ann. Chem.*, **35**, 281 (1840).
83. D. Aurbach, M. L. Daroux, P. W. Faguy, and E. Yeager, *J. Electrochem. Soc.*, **134**, 1611 (1987).
84. R. Dedryvère, L. Gireaud, S. Grugeon, S. Laruelle, J.-M. Tarascon, and D. Gonbeau, *J. Phys. Chem. B*, **109**, 15868 (2005).
85. G. V. Zhuang, H. Yang, P. N. Ross, K. Xu, and T. R. Jow, *Electrochem. Solid-State Lett.*, **9**, A64 (2006).
86. G. Zhuang, Y. Chen, and P. N. Ross, *Surf. Sci.*, **418**, 139 (1998).
87. S. Xu, S. K. Das, and L. A. Archer, *RSC Adv.*, **3**, 6656 (2013).
88. Y. Liu, R. Wang, Y. Lyu, H. Li, and L. Chen, *Energy Environ. Sci.*, **7**, 677 (2014).
89. X. Li, S. Yang, N. Feng, P. He, and H. Zhou, *Chinese J. Catal.*, **37**, 1016 (2016).
90. Y. Qiao, J. Yi, S. Wu, Y. Liu, S. Yang, P. He, and H. Zhou, *Joule*, **1**, 359 (2017).